Journal of Materials Chemistry

Cite this: J. Mater. Chem., 2011, 21, 13627

www.rsc.org/materials

PAPER

Composites of quaternized poly(pyridylacetylene) and silver nanoparticles: Nanocomposite preparation, conductivity and photoinduced patterning†

Yu Mao,[a] Hai Peng Xu,[a] Hui Zhao,[a] Wang Zhang Yuan,[ab] Anjun Qin,[ab] Yong Yu,[b] Mahtab Faisal,[b] Zhang Xiao A,[a] Jing Zhi Sun*[a] and Ben Zhong Tang*[ab]

Received 7th April 2011, Accepted 15th June 2011
DOI: 10.1039/c1jm11459j

Suspensions containing quaternized poly(pyridylacetylene) (PPyA) and AgX (X = Br and I) were obtained by simply mixing PPyA with water soluble silver salts. The suspensions were stable in the dark at room temperature, and could be cast into uniform films. After exposure to UV-light for sufficient time, Ag nanoparticles were *in situ* generated in the polymer matrix *via* photochemical reaction. By adjusting the Ag^+ contents and the halide counterions, the size of Ag particles, the conductivity of the composite films, and the surface morphology of the composites were tuned. The quaternized PPyA absorbed UV-light efficiently and the photogenerated halogen caused fast degradation of the polymers. Thus the photo-chemical process concomitantly resulted in the formation of Ag nanoparticles and highly porous films. These properties offer the composite materials potential in the construction of UV-eroding conductive patterns, embedded metal nanostructures, and porous films for loading metal particles as catalyst.

Introduction

Composites of metal-nanoparticles dispersed in polymeric materials are of great interest from both fundamental and technological aspects, as their fine control and design lead to the fabrication of materials with interesting electronic, optical, magnetic, and catalytic properties.[1–4] In the fabrication of the composite materials, the methodology of incorporating metal nanoparticles into a polymer matrix plays a key role. A simple and direct strategy is blending the as-prepared metal nanoparticles with polymers, but these composite materials are often formed far from equilibrium inducing coalescence processes of the metal clusters, and the stability of the composites is undesirable. In an alternative process, monomers are *in situ* polymerized on the surface of or around the entities of preformed metal-nanoparticles.[2a,b,5–8] In this methodology, metal-nanoparticles are formed within the polymer matrices from preset metal precursors. Usually, the process involves the binding or chelating of functional groups of polymers with metal cations from solution, and the formation of the nanoparticles results from the chemical/physical treatment. Through chemical reduction or photochemical reaction, the metal cations are transformed into metal atoms and nucleate and grow into nanoparticles within the polymer matrices; thus the expected polymer/metal-nanoparticles composites are obtained.

Another widely used approach is the synthesis of metal-nanoparticles inside multilayered thin films prepared by the sequential deposition of polyelectrolytes *via* layer-by-layer (L*b*L) assembly.[9–15] In this method, multilayered polyelectrolyte films are immersed into aqueous solutions containing metal cations, where the metal cations bind to the functionalities such as carboxylic acid, sulfonic acid, and amino groups. The *in situ* formation of metal nanoparticles is induced by successive chemical or photochemical reactions. The L*b*L assembly process can also be directly used in the construction of metal-nanoparticles-embedded multilayered thin films by assembling polyelectrolyte and preformed metal-nanoparticles bearing opposite surface charge.[16] These approaches result in polymer/metal-nanoparticles composites characterized by a sandwich structure containing alternative metal-nanoparticle and polymer layers. In principle, the methodologies of L*b*L self-assembling and simultaneous synthesis of metal-nanoparticle and polymer merit the following advantages. Firstly, both approaches demonstrate stable dispersion of metal-nanoparticles in the polymer matrix because of the limited porous feature of polyelectrolyte films and confined diffusion of metal-nanoparticles by surrounding polymer chains. Secondly, by controlling the deposition conditions

[a]*Institute of Biomedical Macromolecules, MOE Key Laboratory of Macromolecular Synthesis and Functionalization, Department of Polymer Science and Engineering, Zhejiang University, Hangzhou, 310027, P. R. China. E-mail: sunjz@zju.edu.cn; Fax: +86-0571-87953734; Tel: +86-0571-87953734*
[b]*Department of Chemistry, The Hong Kong University of Science & Technology, Clear Water Bay, Kowloon, Hong Kong, P. R. China. E-mail: tangbenz@ust.hk; Fax: +852-2358-7375; Tel: +852-2358-1594*

† Electronic supplementary information (ESI) available: Characterization spectra of PyA, PPyA, PPyA–MI and PPyA–MBr (in DMSO), PPyA–$MeBr^-[Ag(NH_3)_2]NO_3$ (in water); Fluorescence spectra of PPyA (in DCM and methanol) and PPyA–MI (in water); and a typical surface elementary analysis of the casting film of PPyA–MBr/$[Ag(NH_3)_2]NO_3$ composite. See DOI: 10.1039/c1jm11459j

such as the species of the metal cations and the binding of functional groups on polymer chains, various polymer/metal-nanoparticles composites can be designed and prepared; thereby nanocomposites showing various physical and chemical properties can be derived.

In the preparation of polymer/metal nanocomposites, the choice of polymer also plays a crucial role. Ranging from block-copolymers,[6e,17] polyelectrolyte,[10–16,18,19] to conjugated polymers and oligomers, a variety of polymers for the fabrication of polymer/metal-nanoparticle composites have been reported. Among these polymers, conjugated polymers are particularly intriguing, because they have π-conjugated backbones, which bestow the polymers with remarkable electronic and optical properties. R. Gangopadhyay and A. De contributed a review on conducting polymer nanocomposites in 2000,[3] Sih and Wolf presented a detailed summary of nanocomposites of conjugated polymers and metal nanoparticles in 2005,[4] and more recently, significant progress has been achieved.[20–30] An elegant example is the research on the preparation and properties of conjugates of poly(phenylene vinylene)s (OPVs) derivatives and gold nanoparticles.[20–23] Schenning and colleagues demonstrated a principle for organization of metal/π–conjugated nanoparticles involving self-assembly of peripheral π–conjugated ligands. Through non-covalent interactions between gold and disulfide[21,22c] or pyridyl[22a,c] moieties, the self-assembled nanoparticles rendered improved stability and controllable morphology in comparison with the products obtained by direct mixing preformed metal-nanoparticles with suitable π–conjugated oligomers and polymers. Fractal-like objects observed in dentritic π–conjugated systems,[21a,22a] hybrids of π–conjugated OPV tapes and gold nanoparticles,[21b,22a] chain-like networks[22a] were derived by tuning the structure of the π–conjugated ligands, the size of the gold nanoparticles and the compositions.[21–23]

Polyacetylene is the prototypical conjugated polymer, its functional derivatives have shown versatile properties such as electrical and photoconductivity, liquid crystal property, gas permeability, chiral recognition, supramolecular assemblies, formation of helical graphitic nanofibers, which have been comprehensively reviewed in the literature.[24,25] We synthesized a series of functional polyacetylenes and prepared their composites with inorganic components including perovskite structures,[26] CdS nanorods,[27,28a] inorganic semiconductor nanoparticles,[28] and carbon nanotubes.[28b,29,30] A representative work was the decoration of multiwalled carbon nanotubes (MWNTs) by Ag nanoparticles with the aid of an amino-functionalized polyphenyacetylene (PPA).[28b] In this case, the amino-functionalized PPA was mixed with MWNTs in an acid media and afforded PPA/MWNT nanohybrids. The polymer chains wrapping on the surface of MWNTs furnish the surface with numerous amino groups, which further attract Ag^+ cations. By chemical reduction of Ag^+ cations, Ag nanoparticles were decorated on the surface of MWNTs.

Herein, we report an alternate strategy to fabricate polyacetylene/Ag nanocomposites by rational design. The polyacetylenes used here are quaternized poly(pyridyl–acetylene) (PPyA–MI, X = Br and I, Chart 1).[31] Through simply mixing PPyA–MX with proper water-soluble silver salts, the chemical reaction of halide anions with Ag^+ cations afford AgX particles

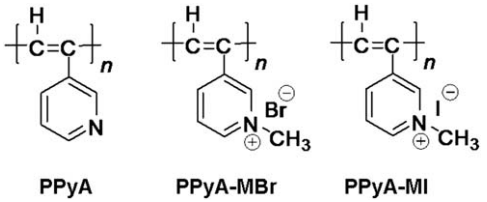

Chart 1 Chemical structure of polyacetylene derivatives.

and charged $[Ag_nI_m]$ clusters in the mixtures.[32] Exposure to UV-light, enables the Ag nanoparticles to be *in situ* generated in the polymer matrix and nanocomposites of polymer/Ag particles can be fabricated. Then, morphological features and electrical properties of the composites were investigated.

Results and discussion

Formation of polymer/Ag nanocomposites

The synthesis and characterization of the polymers are described elsewhere[31] and some characterization data are included ESI (Fig. S1 to S5†). The synthetic route to composites of PPyA–MX/Ag nanoparticles is shown in Scheme 1, and the preparation of the PPyA–MI/Ag composite is as follows. When $AgNO_3$ aqueous solution was added to the PPyA–MI dimethylsuloxide (DMSO) solution containing stoichiometric amounts of solute, the Ag^+ cations immediately reacted with I^- anions and AgI precipitate formed readily. Due to the strong polarization effect of Ag^+ cations, the AgI particles were negatively charged by excess I^- anions. As a result, charged $[Ag_nI_m]$ clusters formed in the mixture and polycationic PPyA–M^+ macromolecules were attracted to the cluster surroundings.[32] Thanks to the ionic repulsion interaction between cationic polymer chains, the particles did not aggregate further, and the resultant suspension was quite stable. For proper Ag^+:I^- ratios, no precipitate was observed when the mixture was kept in the dark for 9 months. Once exposed to UV light the dark yellow suspension turned black-brown. The color change is associated with the formation of Ag nanoparticles due to UV-induced decomposition of AgI and/or $[Ag_nI_m]$ clusters.

To observe the morphology of AgI particles and $[Ag_nI_m]$ clusters in the suspension, thin films were cast on TEM micro-grids from the as-prepared suspension. To our surprise, for some composite films, no evident particle-like morphology was observed at first, but dentritic black traces came into view under the irradiation of electron beams. This phenomenon is ascribed to the formation of Ag nanoparticles in the film. Fig. 1 displays typical TEM images recorded for a composite film in which the

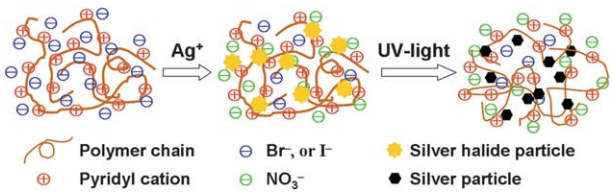

Scheme 1 Preparation of the composites of PPyA–MX/Ag nanoparticles.

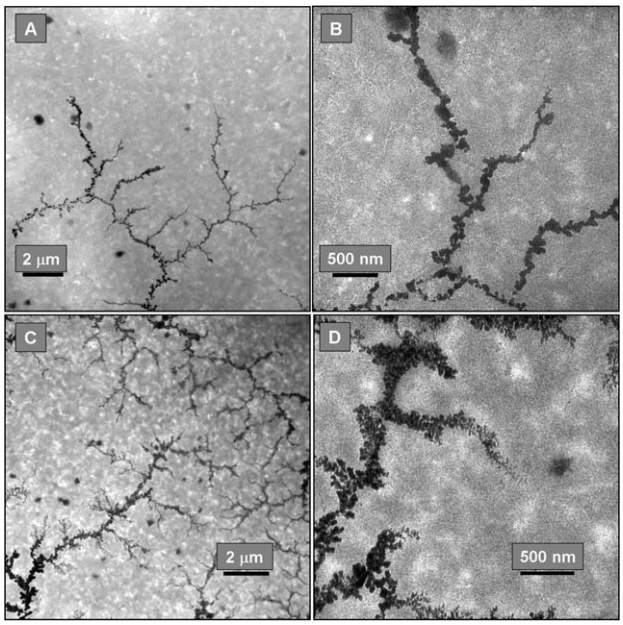

Fig. 1 TEM images of the composite films of PPyA–MI/$AgNO_3$ (Ag^+:I^- = 1:2, by mole) under exposure to electron beams. The exposure times for (A) and (C) are 3 and 10 s, respectively; (B) and (D) are magnified images of (A) and (C), respectively.

molar ratio of Ag^+:I^- is 1:2. The dentritic black trails formed quickly upon the electron beam irradiation, in just 3 s as indicated in Fig. 1A. The trails grew thicker and more trails emerged in the field of vision with the extension of exposure time (Fig. 1A–C). A magnified image Fig. 1C clearly displays trails composed of smaller black particles (Fig. 1D). These trails present a vivid picture showing the propagation of Ag nanoparticles' networks and the percolation path in the polymer matrix.

It is well-known that Ag can also be derived by photochemical reduction of AgI. Thus we tried to generate *in situ* Ag particles in $AgNO_3$/PPyA–MI composites. The TEM images in Fig. 2 show the typical morphology of the generated particles. These images were taken from composite films cast from suspensions after exposure to UV light for 12 h. The absence of dentritic trails indicates that the AgI component had been largely reduced to Ag by UV-irradiation. When content of the Ag^+ component in the composite was lower, for example, the molar ratios of Ag^+:I^- were 2:10 and 3:10, black nanoparticles were observed. An important feature found at low Ag^+:I^- molar ratios is that the particles have smaller sizes. For the composite of Ag^+:I^- = 2:10, the average size of the Ag particles is 20 nm (Fig. 2A). With increasing Ag^+ content, the size of the particles grows larger. When the composite of Ag^+:I^- is 5:10 (or 1:2), the average size of the Ag particles is about 150 nm (Fig. 2B). Further increasing the Ag^+ content leads to an even larger particle size; particles in diameter of 500 nm can be observed in the case that the composite of Ag^+:I^- is 7:10 (Fig. 2C). Another feature shown in Fig. 2 is that the particles' size distribution is relatively narrow at low Ag^+ component content, as revealed by Fig. 2A and B. When the ratio of Ag^+:I^- is over 1:2, the size distribution becomes broader. Meanwhile, particles are irregular in shape (see Fig. 2C and 2D).

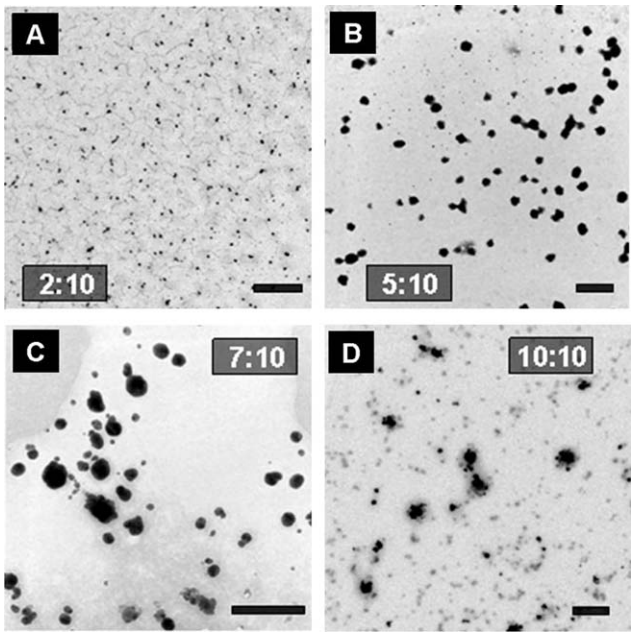

Fig. 2 TEM images of Ag nanoparticles formed in the composites of PPyA–MI/$AgNO_3$ with different ratios of Ag^+:I^-. Scale bar: 1 μm.

The above-mentioned features can be explained as following. Low Ag^+ content indicates low local Ag^+ concentration but relatively high I^- concentration. Meanwhile, low Ag^+ content means that the concentration of polymer is relatively high. Consequently, charged [Ag_nI_m] clusters are formed and they are surrounded by thicker polymer components, which restrain the diffusion of Ag^+ and charged [Ag_nI_m] clusters. These two factors together result in the formation of small AgI particles and [Ag_nI_m] clusters at low Ag^+ contents. Thus small Ag particles are generated *in situ* in the polymer matrix. The "huge" polymer surrounding also restrains the aggregation of the Ag particles, and uniform distribution of the particles has been observed. The static electric repulsion between charged [Ag_nI_m] clusters and the restraining effect of the polymer component are confirmed by the fact that the composite suspensions with low Ag^+ content (Ag^+:I^- is lower than 1:2) can be stored for over ten months in the dark at room temperature. In contrast, at high Ag^+ content, larger AgI particles and [Ag_nI_m] clusters can form due to the more plentiful Ag^+ and I^- supplying and the weaker restraining feature of the surrounding polymer component. In addition, quick formation of AgI particles and weak polymer obstruction to particle aggregation lead to the formation of irregular particles, which in turn leads to the irregular size and shape of the final Ag particles.

The suspensions of PPyA–MBr/$AgNO_3$ composites behave differently from the PPyA–MI/$AgNO_3$ system. Even at low Ag^+ content, the suspension was instable and precipitate formed after being kept in the dark for days. This may be attributed to the fact that [Ag_xBr_y] clusters are not as stable as [Ag_nI_m] clusters. To solve this problem, we transferred Ag^+ to $Ag(NH_3)_2^+$ before mixing with the PPyA–MBr component. Fortunately, the resulting suspension showed improved stability at low Ag^+ content and the suspension was sustained without precipitate for months. Moreover, the thin films cast from the suspensions showed similar behavior under irradiation of electron beams and

UV-light. As shown in Fig. 3A, dentritic trails could be observed in the casting films under the irradiation of electron beams for 3 s; and at the same time, quite a few particles could also be found. This observation indicates the UV-induced photochemical reduction of AgBr is faster than that of AgI. After exposure to UV-light for 1.5 h, Ag nanoparticles were generated in the composite films (Fig. 3B). Because volatile Br_2 was released during the photochemical process, a process harmful to the TEM instrument, further detection of the morphology for longer times and in other samples were limited.

Conductive property of the composite films

Polyacetylene in doping states was the first conducting polymer or synthetic metal showing metallic conductivity. But doped polyacetylenes are both instable and intractable. Substituted polyacetylenes gained better processability and improved stability, but lost electrical conductivity. Incorporating metal particles into host polymers is an effective strategy to fabricate electrical conductive plastic films. According to the literature, *in situ* generation of metal particles in polymer matrix shows some advantages such as sufficient dispersion, uniform size distribution and better polymorphous stability.[3,4] As described above, Ag nanoparticles can be photochemically generated in PPyA–MI and PPyA–MBr matrices. It is conceivable that the composites films containing Ag nanoparticles should have improved electrical conductivity.

To confirm this hypothesis, we examined the electrical conductivity of the casting films after sufficient exposure to UV-light. The typical *I–V* curves for the composite films containing different amounts of Ag are shown in Fig. 4. The primary polymer PPyA has the worst conductivity, which is weaker than the lower limit (10^{-9} S cm^{-1}) of the apparatus. The quaternized polymer PPyA–MI shows higher conductivity; the electric density of the PPyA–MI film at 1.5 V bias is about 3 times that of the PPyA film at the same bias. Such an enhancement may come from the mobile I^- species in the PPyA–MI film and/or the extension of π–conjugation in PPyA–MI in comparison with PPyA (see Fig. S4†). When Ag nanoparticles are generated in the films, the current density grows steeply. For the composite whose molar ratio of Ag^+:I^- is 1:5 (2:10, the curve symbolized by open up-triangles, Fig. 4), at 1.5 V bias, the casting films show an

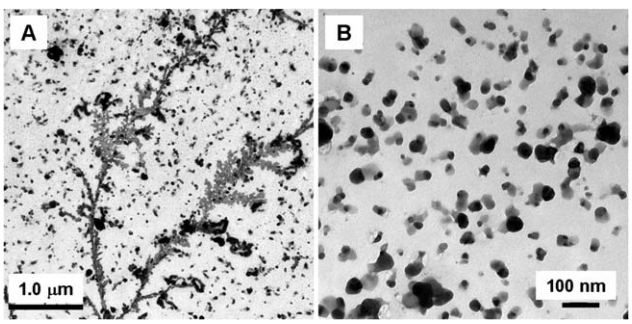

Fig. 3 (A) A typical TEM image of dentritic trails formed in the composite film of PPyA–MBr/$Ag(NH_3)_2NO_3$ under irradiation of electron beams for 3 s. (B) A TEM image of the Ag nanoparticles generated in a casting film of PPyA–MBr/$Ag(NH_3)_2NO_3$; the ratio of Ag^+:Br^- is 1:2, and the time for UV-irradiation was 1.5 h.

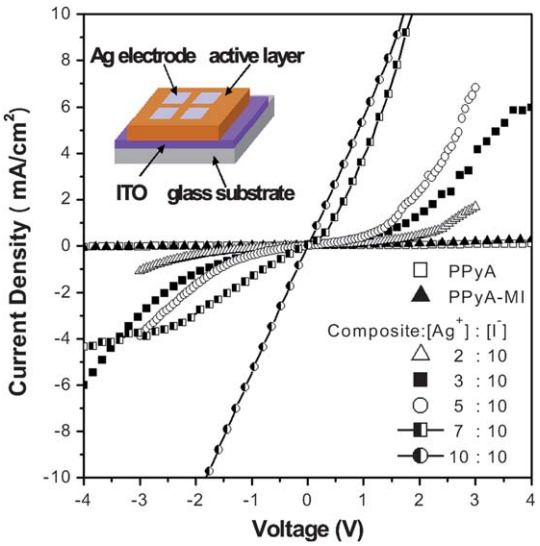

Fig. 4 *I–V* curves of PPyA, PPyA–MI and PPyA–MI/Ag composites films composing of different ratios of Ag^+:I^-. Inset is the schematic configuration of the device used for *I–V* curve measurement.

average current density that is about 11 times higher than the data recorded for PPyA casting films. At the same bias, the amplification is increased to about 50 when the molar ratio of Ag^+:I^- is 1:2 (5:10, open circle). Further increasing the molar ratio of Ag^+:I^- to 1:1 (10:10, shadow-circle), the current intensity is boosted up to over 500 times of the casting films of PPyA, and the conductivity is approximate to 10^{-6} S cm^{-1}, falling into the region of semiconductor. For these films, the *I–V* curves are straight lines, indicating a standard ohmic behavior, rather than a rectifying performance of semiconductors.

The composite suspensions of PPyA–MBr and $Ag(NH_3)_2NO_3$ were also cast to fabricate thin films on ITO glass substrates. But after exposure to UV-light for hours, the films became cracked. Huge fluctuations in data were recorded in the measurements, which could not be used to evaluate the conductivity. A possible reason was that the photo-chemically generated bromide randomly destroyed the conductive layer on ITO glass as well as the polymer matrix. This deduction was directly approved by the optical photographs taken from the casting films on quartz plates. As revealed by the images in Fig. 5, the casting film of the intrinsic PPyA–MBr exhibits a smooth surface. After introduction of Ag^+ species into the PPyA–MBr solution, the casting film (Ag^+:Br^- = 1:2) shows a coarse surface; tiny clusters scatter all over the surface of the image. But after exposure to UV-light for

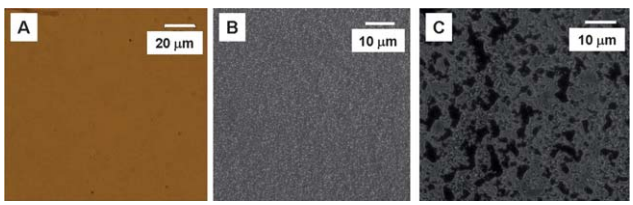

Fig. 5 Optical images showing the surface morphology of PPyA–MBr casting film (A), PPyA–MBr/$(NH_3)_2NO_3$ composite film (B), and the composite film after exposure to UV-light for 1.5 h.

1.5 h, the surface morphology of the film is characterized by larger particles dispersing in polymer matrix like isolated islands and their sizes grew into several micrometres.

To get more detailed information about the morphological features of the PPyA–MBr/Ag composite films, we observed the morphology changes occurred to the casting films by atomic force microscope (AFM). As shown in Fig. 6A, the surface of the film is quite smooth, and the maximum fluctuation is only about 5 nm. After the formation of AgBr particles in the suspension, the surface of the casting films becomes rough, and the roughness can be evaluated by the maximum fluctuation, which is about 130 nm in a dimension of 10 μm × 10 μm (Fig. 6D). When the film was exposed to UV-light for 1.5 h, the surface were too fluctuated to be scanned by AFM probe.

Photoinduced patterning of composite films

The failing to probe the surface morphology of the casting films by AFM and the images in Fig. 3 and 6 imply that the UV-light disrupts the composites. This led to the idea of making patterns by taking the advantage of the photo-induced decomposition. The experiment results are displayed in Fig. 7. Square grid-like patterns were formed when UV-light irradiated through a metal mask to the casting film of PPyA–MBr on quartz plate. Both shadow and shadow-free parts present smooth surface; the spots on the surface may be dust particles from atmosphere. The shallow square troughs corresponding to the shadow-free part were produced by UV-light induced decomposition of the polymer and cross-linking of the polyene backbones, which caused the volume shrinking of the polymer matrix. Remarkably

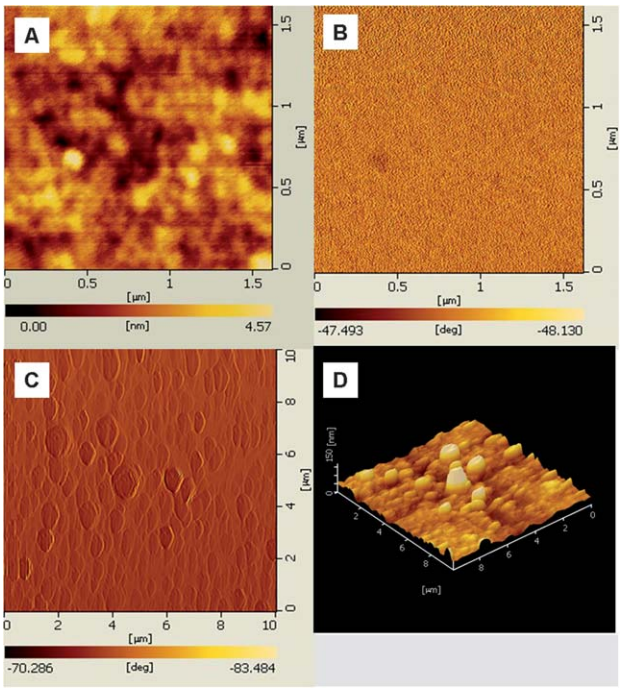

Fig. 6 AFM images showing the surface morphology of casting film of PPyA–MBr/Ag$(NH_3)_2NO_3$ composite. (A) Before exposure to UV-light, probed in tapping mode, (B) in phase mood; (C) After exposure to UV-light for 1.5 h, probed in phase mood, (D) three dimensional image recorded for the same area of image C in tapping mood (Br^-:Ag = 1:2).

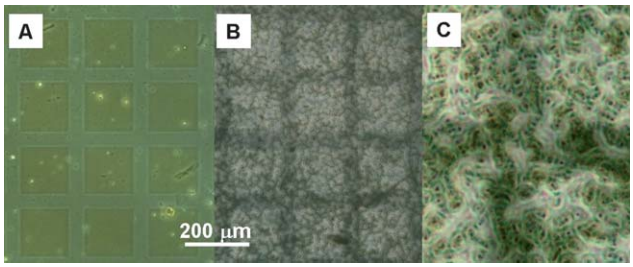

Fig. 7 Optical images showing the surface morphology of PPyA–MBr casting films (A), PPyA–MBr/Ag$(NH_3)_2NO_3$ composite film (B) after exposure to UV-light for 1.5 h, (C) magnified image showing the texture from (B).

different from casting film of PPyA–MBr, after irradiation by UV-light for 1.5 h, the surface of composite film (Ag^+:Br^- = 1:2) presents a typical morphology characterized by wire-like veins, particle-like nets and pores. The hugely fluctuated and highly porous surface made it unworkable for AFM probe. Elementary analysis indicates Ag, Br, N elements are present on the surface of the film, and the enrichment of Ag is higher than that of Br (see Fig. S5†). These results together with the observation shown in Fig. 7 confirm the existence of Ag particles in the films. The Ag/Ag^+ species may catalyze the oxidation of Br^- to bromide, which accelerates the decomposition of the polymer. Thus a morphology shown in Fig. 6D, Fig. 7B and 7C exists. The coexistence of Ag particles and highly porous structure is favorable for the construction of highly efficient catalyst systems.

Conclusions

In summary, we have demonstrated the preparation of the composites of quaternized poly(pyridylacetylene) and Ag nanoparticles, the electrical properties, and the photo-induced patterning of the casting films of the nanocomposites. By simply mixing the DMSO solution of PPyA–MI with aqueous solution containing stoichiometric amounts of $AgNO_3$ (PPyA–MBr with Ag$(NH_3)_2NO_3$), uniform suspensions were obtained. The suspensions were quite stable at low Ag^+ content (Ag^+:X^- < 1:2, X = I or Br); no precipitate was observed when kept in dark and at low temperature for months. Uniform films were fabricated by casting the suspensions onto quartz substrates. Both optical microscopic and AFM images showed that the surface of the casting films were smooth. When exposed to electron beam during TEM measurements, black dentritic trails propagated in the films, and the propagation rate in composite films of PPyA–MBr/Ag$(NH_3)_2NO_3$ was higher than that in PPyA–MI/$AgNO_3$. Meanwhile, Ag nanoparticles were generated in the composites due to photochemical reduction of AgX to Ag. This reduction process was also fulfilled by exposing the casting films or the suspensions to UV-light for hours, much easier and safer when compared to exposure to the electron beam. TEM images clearly demonstrate that the particle size is small and the size distribution is narrow at lower Ag^+ content, while size distribution becomes wider and the particle size becomes larger at higher Ag^+ content. These results indicate that the composites of poly(*meso*-pyridylacetylene)s and Ag nanostructures can be derived from *in situ* generation of Ag nanoparticles *via* a facile photochemical

route, and the morphology of the Ag component can be tuned by tuning the composition.

When the ratio of Ag^+ and I^- was higher than 1:2, the casting films containing photochemically generated Ag particles showed a remarkable increase in electrical conductivity. This was ascribed to the formation of electron percolation paths in the films when enough amounts of Ag particles were photo-chemically generated. The conductivity in the semiconductor region approached (10^{-6} S cm^{-1}), and the *I–V* curve indicated ohmic conducting behavior. For the composites of PPyA–MBr/Ag $(NH_3)_2NO_3$, UV-irradiation induced quick generation of Ag particles and decomposition of the composites. The Ag/Ag^+ catalyzed process is a rational mechanism because of the high oxidation activity of the photo-generated Br_2. The UV-light induced Ag formation and polymer decomposition resulted in a highly porous surface embedded with Ag nanoparticles. These morphological features and properties observed for composites of polyacetylenes and Ag nanostructures are distinct from those reported for the composites of non-conjugated polymer and Ag nanoparticles. They offer composite materials with potential uses in the construction of UV-eroding conductive patterns, implant metal nanostructures, porous and patterned catalyst arrays, as well as versatile high-technology applications.

Experimental

Chemicals and materials

Dimethylsulfone (DMSO) and $AgNO_3$ were both in AR grade and purchased from the National Chemicals Co. Ltd., Shanghai, China; $Ag(NH_3)_2NO_3$ was prepared by mixing 0.1 mol L^{-1} $AgNO_3$ aqueous solution with saturated ammonia. The quaternized poly(pyridylacetylenes) were prepared in our laboratory and structural characterization data are reported elsewhere.[31]

Instrumentation

^1H and ^{13}C NMR spectra were measured on a Bruker AV 400 spectrometer. Absorption spectra were measured on a Varian CARY 100 Bio UV-visible spectrophotometer. Fluorescence spectra were recorded on a Perkin-Elmer LS 55 spectrofluorometer. Transmission electron microscope (TEM) photographs were recorded with a JEOL 100CX TEM at an accelerating voltage of 100 kV. Surface morphology of the casting films was monitored on a PicoPlus SPM 3800 aparatus. Photochemical reduction of the silver cations in the casting films or suspensions was carried out under the UV-irradiation with an intensity of 18.5 mW cm^{-2} at 365 nm. The current–voltage (*I–V*) curves were recorded on Agilent Technologies 4155C Semiconductor Parameter Analyzer; the film thickness was controlled at 1 to 1.5 μm. The bottom contact was ITO glass and the top contact was a silver layer deposited *in vacuo* onto the composite layer in a size of 2 × 3 mm^2.

Preparation of hybrids of polymer/Ag nanoparticles

In a series of 5 mL vials, 15 mg PPyA–MI and 1 mL DMSO were added. In another 5 mL vial, 105 mg silver nitrate ($AgNO_3$) was dissolved in 1 mL deionized water. Then 20, 30, 50, 70, and 100 μL $AgNO_3$ aqueous solution was introduced into each vial containing DMSO solution of PPyA–MI. Stirring obtained a uniform suspension, which was exposed to UV light irradiation for 1.5 h. Ag particles were generated by photo-chemical reduction of AgI in the suspension. The obtained hybrids of polymer/Ag particles were sent for TEM observation, thermal property measurement, and film casting. Films of polymers and the hybrids of methyl-quaternized polymer/Ag particles were solution-cast onto the surface of pretreated conductive glass plates (ITO, indium–tin oxides coating on glass). The thickness of the films for electrical conductivity measurement was controlled to 1.0 to 1.5 μm.

Characterization data of *PPyA–MBr*

The characterization data for PyA, PPyA and PPyA–MI are reported elsewhere.[31] Some of the data are included in Fig. S1, S2, S3, S4 and S5† for comparison with PPyA–MBr. PPyA–MBr was obtained as a dark brown solid in a yield of 92.2%. ^1H NMR (300 MHz, D_2O), δ (TMS, ppm): 8.91 (Pyridnie-***H***, at 2 position), 8.41 (Pyr-***H***, at 4 and 6 positions), 7.85 (Pyr-***H***, at 5 position), 6.52 (***H***C═), 4.13 (CH_3). ^{13}C NMR (400 MHz, D_2O), δ (TMS, ppm): 146–125 (Pyr-***C***, at 2, 3, 4, 5, and 6 positions; HC═***C***Pyr), 48 (***C***H_3).

Acknowledgements

This work was partially supported by the National Science Foundation of China (21074113, 50873086, 20634020 and 20974028); the Research Grants Council of Hong Kong (603509 and HKUST2/CRF/10), and the University Grants Committee of Hong Kong (AoE/P-03/08). B.Z.T. thanks Cao Guangbiao Foundation of Zhejiang University for its support.

Notes and references

1 A. Heilmann, *Polymer Films with Embedded Metal Nanoparticles*, Spinger, Berlin, 2003.
2 Example of recent reviews, (*a*) G. V. Ramesh, S. Porel and T. P. Radhakrishnan, *Chem. Soc. Rev.*, 2009, **38**, 2646; (*b*) Y. Ofir, B. Samanta and V. M. Rotello, *Chem. Soc. Rev.*, 2008, **37**, 1814; (*c*) J. Shan and H. Tenhu, *Chem. Commun.*, 2007, 4580; (*d*) M. Aizawa and J. M. Buriak, *Chem. Mater.*, 2007, **19**, 5090.
3 R. Gangopadhyay and A. De, *Chem. Mater.*, 2000, **12**, 608.
4 B. C. Sih and M. O. Wolf, *Chem. Commun.*, 2005, 3375.
5 Examples for polymer-Ag composites, (*a*) W. Fritzsche, H. Porwol, A. Wiegand, S. Bornmann and J. M. Köhler, *Nanostruct. Mater.*, 1998, **10**, 89; (*b*) A. S. Korchev, M. J. Bozack, B. L. Slaten and G. Mills, *J. Am. Chem. Soc.*, 2004, **126**, 10; (*c*) S. Rifai, C. A. Breen, D. J. Solis and T. M. Swager, *Chem. Mater.*, 2006, **18**, 21; (*d*) J. Li, K. Kamata, S. Watanabe and T. Iyoda, *Adv. Mater.*, 2007, **19**, 1267; (*e*) A. M. B. Silva, C. B. de Araujo, S. Santos-Silva and A. Galembeck, *J. Phys. Chem. Solids*, 2007, **68**, 729; (*f*) R. D. Deshmukh and R. J. Composto, *Chem. Mater.*, 2007, **19**, 745; (*g*) T. Hasell, L. Lagonigro, A. C. Peacock, S. Yoda, P. D. Brown, P. J. A. Sazio and S. M. Howdle, *Adv. Funct. Mater.*, 2008, **18**, 1265.
6 Examples for polymer-Au composites, (*a*) J. Won, K. J. Ihn and Y. S. Kang, *Langmuir*, 2002, **18**, 8246; (*b*) B. Sohn, B. Seo and S. Yoo, *J. Mater. Chem.*, 2002, **12**, 1730; (*c*) S. Porel, S. Singh and T. P. Radhakrishnan, *Chem. Commun.*, 2005, 2387; (*d*) A. Pucci, M. Bernabo, P. Elvati, L. I. Meza, F. Galembeck, C. A. de Paula Leite, N. Tirelli and G. Ruggeriab, *J. Mater. Chem.*, 2006, **16**, 1058; (*e*) J. Zhang, Y. Gao, R. A. Alvarez-Puebla, J. M. Buriak and H. Fenniri, *Adv. Mater.*, 2006, **18**, 3233; (*f*) M. Sakamoto, T. Tachikawa, M. Fujitsuka and T. Majima, *Adv. Funct. Mater.*, 2007, **17**, 857.

7 (*a*) S. Porel, N. Hebalkar, B. Sreedhar and T. P. Radhakrishnan, *Adv. Funct. Mater.*, 2007, **17**, 2550; (*b*) S. Porel, N. Venkatram, D. N. Rao and T. P. Radhakrishnan, *J. Appl. Phys.*, 2007, **102**, 033107; (*c*) S. Horiuchi and Y. Nakao, *Curr. Nanosci.*, 2007, **3**, 206; (*d*) Y. Lee, J.-R. Choi, K. J. Lee, N. E. Stott and D. Kim, *Nanotechnology*, 2008, **19**, 415604; (*e*) M. Harada and Y. Inada, *Langmuir*, 2009, **25**, 6049.

8 C. Mendoza, T. Pietsch, J. S. Gutmann, D. Jehnichen, N. Gindy and A. Fahmi, *Macromolecules*, 2009, **42**, 1203.

9 L. Shang, Y. Wang, L. Huang and S. Dong, *Langmuir*, 2007, **23**, 7738.

10 P. J. G. Goulet, Jr, D. S. dos Santos, R. A. Alvarez-Puebla, Jr, O. N. Oliveira and R. F. Aroca, *Langmuir*, 2005, **21**, 5576.

11 M. Vago, M. Tagliazucchi, F. J. Williams and E. J. Calvo, *Chem. Commun.*, 2008, 5746.

12 (*a*) D. M. DeLongchamp and P. T. Hammond, *Chem. Mater.*, 2003, **15**, 1165; (*b*) J. L. Lutkenhaus, K. McEnnis and P. T. Hammond, *Macromolecules*, 2008, **41**, 6047.

13 (*a*) S. Joly, R. Kane, L. Radzilowski, T. Wang, A. Wu, R. E. Cohen, E. L. Thomas and M. F. Rubner, *Langmuir*, 2000, **16**, 1354; (*b*) T. C. Wang, M. F. Rubner and R. E. Cohen, *Langmuir*, 2002, **18**, 3370; (*c*) K.-K. Chia, R. E. Cohen and M. F. Rubner, *Chem. Mater.*, 2008, **20**, 6756.

14 (*a*) J. Dai and M. L. Bruening, *Nano Lett.*, 2002, **2**, 497; (*b*) E. Geraud, H. Möhwald and D. G. Shchukin, *Chem. Mater.*, 2008, **20**, 5139.

15 (*a*) B. L. Rivas and C. Muñoz, *J. Appl. Polym. Sci.*, 2009, **114**, 1587; (*b*) E. Veletanlic and M. C. Goh, *J. Phys. Chem. C*, 2009, **113**, 18020.

16 L. E. Russell, A. A. Galyean, S. M. Notte and M. C. Leopold, *Langmuir*, 2007, **23**, 7466.

17 (*a*) W. A. Lopes and H. M. Jaeger, *Nature*, 2001, **414**, 735; (*b*) B. Sohn, B. Seo and S. Yoo, *J. Mater. Chem.*, 2002, **12**, 1730; (*c*) L. Wang and Y. Yamauchi, *J. Am. Chem. Soc.*, 2009, **131**, 9152.

18 B. Harnish, J. T. Robinson, Z. Pei, O. Ramstrom and M. Yan, *Chem. Mater.*, 2005, **17**, 4092.

19 D. Li, Q. He, Y. Cui and J. B. Li, *Chem. Mater.*, 2007, **19**, 412.

20 M. Sangermano, Y. Yagci and G. Rizza, *Macromolecules*, 2007, **40**, 8827.

21 (*a*) V. J. Gandubeert and B. Lennox, *Langmuir*, 2005, **21**, 6532; (*b*) G. de La Torre, F. Giscalone, J. L. Segula, N. Martin and D. M. Guldi, *Chem. Eur. J.*, 2005, **11**, 1267.

22 (*a*) J. van Herrikhuyzen, R. A. J. Janssen, E. W. Meijer, S. C. J. Meskers and A. P. H. J. Schenning, *J. Am. Chem. Soc.*, 2006, **128**, 686; (*b*) J. van Herrikhuyzen, S. J. George, M. R. J. Vos, N. A. J. M. Sommerdijk, A. Ajayaghosh, S. C. J. Meskers and A. P. H. J. Schenning, *Angew. Chem., Int. Ed.*, 2007, **46**, 1825.

23 (*a*) X. F. Liu, X. R. He, T. G. Jiu, M. J. Yuan, J. L. Xu, J. Lv, H. B. Liu and Y. L. Li, *ChemPhysChem*, 2007, **8**, 906; (*b*) M. J. Yuan, Y. J. Li, H. B. Liu and Y. L. Li, *Sci. China, Ser. B: Chem.*, 2009, **52**, 715; (*c*) C. H. Li, L. Jiang, H. B. Liu, Y. L. Li and Y. L. Song, *ChemPhysChem*, 2009, **10**, 2058.

24 (*a*) T. Masuda and T. Higashimura, *Acc. Chem. Res.*, 1984, **17**, 51; (*b*) K. Nagai, T. Masuda, T. Nakagawa, B. D. Freeman and Z. Pinnau, *Prog. Polym. Sci.*, 2001, **26**, 721; (*c*) J. W. Y. Lam and B. Z. Tang, *Acc. Chem. Res.*, 2005, **38**, 745; (*d*) J. Z. Liu, J. W. Y. Lam and B. Z. Tang, *Chem. Rev.*, 2009, **109**, 5799.

25 (*a*) K. Akagi, *Chem. Rev.*, 2009, **109**, 5354; (*b*) E. Yashima, K. Maeda, H. Iida, Y. Furusho and K. Nagai, *Chem. Rev.*, 2009, **109**, 6102; (*c*) B. M. Rosen, C. J. Wilson, D. A. Wilson, M. Peterca, M. R. Imam and V. Percec, *Chem. Rev.*, 2009, **109**, 6275.

26 H. P. Xu, J. Z. Sun, A. J. Qin, J. L. Hua, Z. Li, Y. Q. Dong, H. Xu, W. Z. Yuan, Y. G. Ma, M. Wang and B. Z. Tang, *J. Phys. Chem. B*, 2006, **110**, 21701.

27 H. P. Xu, B. Y. Xie, W. Z. Yuan, J. Z. Sun, F. Yang, Y. Q. Dong, A. Qin, S. Zhang, M. Wang and B. Z. Tang, *Chem. Commun.*, 2007, 1322.

28 (*a*) H. P. Xu, J. K. Jin, Y. Mao, J. Z. Sun, F. Yang, W. Z. Yuan, Y. Q. Dong, M. Wang and B. Z. Tang, *Macromolecules*, 2008, **41**, 3874; (*b*) W. Z. Yuan, L. Tang, H. Zhao, J. K. Jin, J. Z. Sun, A. Qin, H. P. Xu, J. Z. Liu, F. Yang, Q. Zheng, E. Chen and B. Z. Tang, *Macromolecules*, 2009, **42**, 52.

29 (*a*) W. Z. Yuan, J. Z. Sun, Y. Q. Dong, M. Häußler, F. Yang, H. P. Xu, A. Qin, J. W. Y. Lam, Q. Zheng and B. Z. Tang, *Macromolecules*, 2006, **39**, 8011; (*b*) W. Z. Yuan, J. W. Y. Lam, A. Qin, J. Z. Sun, Y. Q. Dong, J. Z. Liu, H. P. Xu, Q. Zheng and B. Z. Tang, *Macromolecules*, 2007, **40**, 3159; (*c*) W. Z. Yuan, Y. Mao, H. Zhao, J. Z. Sun, H. P. Xu, J. K. Jin, Q. Zheng and B. Z. Tang, *Macromolecules*, 2008, **41**, 701; (*d*) W. Z. Yuan, J. Z. Sun, J. Z. Liu, Y. Q. Dong, Z. Li, H. P. Xu, A. Qin, M. Haeussler, J. K. Jin, Q. Zheng and B. Z. Tang, *J. Phys. Chem. B*, 2008, **112**, 8896; (*e*) W. Z. Yuan, J. W. Y. Lam, X. Y. Shen, J. Z. Sun, F. Mahtab, Q. Zheng and B. Z. Tang, *Macromolecules*, 2009, **42**, 2523; (*f*) W. Z. Yuan, H. Zhao, X. Y. Shen, F. Mahtab, J. W. Y. Lam, J. Z. Sun and B. Z. Tang, *Macromolecules*, 2009, **42**, 9400.

30 (*a*) H. Zhao, W. Z. Yuan, L. Tang, J. Z. Sun, H. Xu, A. Qin, Y. Mao, J. K. Jin and B. Z. Tang, *Macromolecules*, 2008, **41**, 8566; (*b*) H. Zhao, W. Z. Yuan, J. Mei, L. Tang, X. Q. Liu, J. M. Yan, X. Y. Shen, J. Z. Sun, A. Qin and B. Z. Tang, *J. Polym. Sci., Part A: Polym. Chem.*, 2009, **47**, 4995.

31 Y. Mao, X. A. Zhang, H. Xu, W. Z. Yuan, H. Zhao, A. Qina, J. Z. Sun and B. Z. Tang, *Chin. J. Polym. Sci.*, 2011, **29**, 133.

32 A. Ledo, F. Martinez, M. A. Lopez-Quintela and J. Rivas, *Phys. B*, 2007, **398**, 273.